

All-On-chip Reconfigurable Structured Light Generator

Weike Zhao^{1,#}, Xiaolin Yi^{1,#}, Jieshan Huang², Ruoran Liu¹, Jianwei Wang², Yaocheng Shi¹, Yungui Ma¹, Andrew Forbes^{1,3*} and Daoxin Dai^{1,*}

¹State Key Laboratory for Extreme Photonics and Instrumentation, College of Optical Science and Engineering, Zhejiang University, Hangzhou 310058, China.

²State Key Laboratory for Mesoscopic Physics, School of Physics, Peking University, Beijing 100871, China.

³School of Physics, University of the Witwatersrand, Johannesburg, South Africa.

*Corresponding author: dx dai@zju.edu.cn, Andrew.Forbes@wits.ac.za

#These authors contributed equally to this work: Weike Zhao, Xiaolin Yi

Abstract

Structured light carrying angular momentum, such as spin angular momentum (SAM) and orbital angular momentum (OAM), has been at the core of new science and applications, driving the need for compact on-chip sources. While many static on-chip solutions have been demonstrated, as well as on-chip sources of free-space modes, no architecture that is fully reconfigurable in all angular momentum states and all on-chip has so far been possible. Here we report the first all-on-chip structured light generator for the creation of both scalar and vectorial angular momentum beams, facilitated through a silicon-on-insulator (SOI) chip with a silica mode multiplexer (silica chip). We selectively stimulate six linearly-polarized (LP) modes of the silica multimode bus waveguide, precisely controlling the modal powers and phases with the SOI chip. This allows us to tailor arbitrary superpositions of the mode set thus synthesizing common cylindrical vector vortex beams as well as OAM beams of controlled spin and topological charge. Our compact structured light generator exhibits high switching speed and operates across the telecom band, paving the way for applications such as optical communication and integrated quantum technologies.

Introduction

In recent decades, structured light has captured a great deal of research interest and found a variety of applications¹⁻⁴, including spin angular momentum (SAM) beams^{5,6}, cylindrical vector (CV) beams^{7,8}, orbital angular momentum (OAM) beams^{9,10}, and total angular momentum (TAM)

beams^{11,12}, which have special spatial distributions of intensity, phase or polarization. Among them, SAM beams are associated with circular polarization and carry SAM of $S=\sigma\hbar$ ($\sigma=\pm 1$) per photon, while CV beams feature a circular symmetry polarization distribution and are undetermined at the beam center where there is a polarization singularity. CV beams have shown great potential in various applications, such as plasmonic nanofocusing^{13,14}, particle manipulation¹⁵, and high-resolution optical microscopy¹⁶, due to their unique focusing property. In contrast, OAM beams have a helical phase front characterized by Hilbert factor $\exp(il\theta)$, where l is the topological charge value and θ is the azimuthal angle¹⁷, resulting in a phase singularity at the beam center and an OAM of $l\hbar$ per photon. The unique phase/intensity distribution of OAM beams makes them very useful for widespread applications, including mode-division multiplexing^{18,19}, optical micro-manipulation²⁰⁻²², and optical measurement²³ to name but a few.

The myriad of applications has fuelled the generation of structured light, with the bulk optical toolkit now comprising spatial light modulators^{24,25}, fibre-based devices^{7-9,26-30}, spiral phase plates³¹ and directly from lasers^{32,33}. On-chip structured light generators come with the advantages of compactness, robustness, and versatility, and have attracted significant attention of late. A variety of silicon-on-insulator (SOI) photonic structures have been demonstrated for generating structured light³⁴⁻⁴³. On-chip metamaterials or metasurfaces imply a helical wavefront on the launched light by using a set of meta-atoms that offer a phase modulation of $0-2\pi$ with the principle of electric dipole resonance and generalized laws of reflection/refraction, and have been widely used to emit the OAM beams. By further utilizing the spin-orbit conversion, metamaterial also performs controllable transformation between SAM and OAM beams^{39,40}. Alternatively, holographic gratings, which are compact and efficient, can couple an in-plane guided-mode to a free-space OAM mode by introducing subwavelength surface structures^{41,42}. In addition, dielectric or plasmonic cavities with strong mode coupling have also been developed for on-chip OAM beam generation by using angular gratings to achieve free-space OAM beams with well-controlled topological charges from in degenerate whispering gallery modes (WGM). The different order cavity-modes at discrete resonance wavelengths map to the OAM beams carrying different topological charge values l ⁴³, and the emitting OAM order can be tuned by using an electrical heater³⁸ or utilizing the strong mutual interaction of the SAM and OAM³⁴⁻³⁷. It should be mentioned that the aforementioned schemes are all based on the optical diffraction mechanism,

and their conversion efficiency is limited to $< \sim 25\%$ due to the downward emission to the substrate⁴². A potential solution to improve emission efficiency is coating a reflection layer on the substrate⁴⁴ or adopting unidirectional radiation grating⁴⁵. Furthermore, the large divergence angle of diffraction structures also makes them difficult to be coupled to OAM fibres, which thus hinders their further applications.

More recently, photonic integrated circuits (PICs) have been used to create scalar structured light modes^{46,47}, a nascent direction that holds exciting future promise for structured light generators. In recent advances, the light was injected into the device, amplitude and phase modulated on-chip through a PIC, and then tailored in free-space by interference⁴⁷ or by using a fixed metasurface⁴⁶, producing scalar free-space modes. To realise a compact and reconfigurable approach that extends to arbitrary angular momentum beams that are controlled all on-chip (without free-space coupling) would require engineering spatial modes on the basis of on-chip waveguides or fibres and non-separably combining them with polarisation, in principle allowing all-on-chip reconfigurable angular momentum creation from scalar to vectorial states of SAM and OAM light. While this is highly desirable for fully integrated functionality, it has yet to be realised⁴⁸.

In this paper, we advance the nascent field of PICs as beam creators by demonstrating an all-on-chip reconfigurable structured light generator that produces on-demand angular momentum beams, from scalar vortex beams to vector vortex beams, all as natural fibre modes. We achieve this by using the natural modes of the silica waveguide as our basis set, controlled by six independent outputs of an SOI chip from three ports (each with two orthogonal polarisations), each reconfigurable in modal power and phase. We demonstrate this for a controlled spin and topological charge of OAM modes of order 1, as well as their vectorial combinations, including the well-known cylindrical vector vortex beams, e.g., radially and azimuthally polarised light. Our PIC architecture merges an SOI chip and a silica mode multiplexer (silica chip) for a compact device, while the all-on-chip configuration is ensured by the fibre coupled input and the subsequent on-chip excitation of scalar and vectorial OAM inside the silica multimode bus waveguide (MBW), circumventing the deleterious free-space to chip input/output coupling. Our convenient all-on-chip generation of structured light enjoys fast switching speed, a broad working bandwidth, high conversion efficiency, easy fibre-coupling (input and output), and can be

extended in the future to higher OAM values and arbitrary total angular momentum by simply scaling the SOI chip output ports and MBW size without any fundamental changes to the concept or geometry.

Results

1. Concept and Implementation

Our concept involves the exploitation of the SOI chip for light with controlled amplitude and phase at several output ports, using this to control the superposition of modes in a silica waveguide/fibre by edge coupling, and then finally dynamically adjusting the SOI chip to produce any desired OAM mode directly on a chip within the silica waveguide/fibre by appropriate superposition of the underlying modes. To unpack this by way of example, note that both few-mode fibres (FMFs) and square silica waveguides with appropriate cross-section parameters can support the well-known Linearly Polarised (LP) mode set, with six such LP modes (i.e., LP_{01-x} , LP_{01-y} , LP_{11a-x} , LP_{11a-y} , LP_{11b-x} , and LP_{11b-y}) shown in Fig. 1(a). From these, it is possible to construct, by appropriate superpositions, both scalar and vectorial OAM modes of topological order 1, following³

$$SAM_{\pm 1} = (LP_{01-x} \mp i \cdot LP_{01-y})/\sqrt{2}, \quad (1a)$$

$$RPB = (LP_{11a-x} - LP_{11b-y})/\sqrt{2} \text{ or } (LP_{11a-x} + i \cdot LP_{11b-y})/\sqrt{2}, \quad (1b)$$

$$APB = (LP_{11a-y} - LP_{11b-x})/\sqrt{2} \text{ or } (LP_{11a-y} + i \cdot LP_{11b-x})/\sqrt{2}, \quad (1c)$$

$$OAM_{\pm 1-x} = (LP_{11a-x} \pm i \cdot LP_{11b-x})/\sqrt{2}, \quad (1d)$$

$$OAM_{\pm 1-y} = (LP_{11a-y} \pm i \cdot LP_{11b-y})/\sqrt{2}. \quad (1e)$$

Here the subscript numbers are radial and azimuthal mode orders, a/b is the horizontal/vertical mode azimuth, and -x/-y is the horizontal/vertical polarisation. Higher numbers of LP modes would naturally allow higher-order OAM modes to be engineered. Continuing with our example, we see that the desired modes can be synthesized by selectively combining these six LP modes with specific modal powers and phases, which we achieve with the PIC. For instance, the $SAM_{\pm 1}$ beam can be synthesized by combining the LP_{01-x} and LP_{01-y} modes with a phase difference of $\pi/2$ (for right-handed circular polarization) or $-\pi/2$ (for left-handed circular polarization) according to Eq. (1a), as shown in Fig. 1(b). Note that CV beams contain the radially polarized beam (RPB) and the azimuthally polarized beam (APB), while the RPB and APB can be synthesized with the

LP_{11a} and LP_{11b} modes with different polarizations by following Eq. (1b) and (1c), respectively. The intensity/polarization distributions of the RPB and APB are clearly shown in Fig. 1(c), which both have donut intensity patterns, but are distinguished with radial and azimuthal polarization, respectively. Furthermore, as given in Eq. (1d) and (1e), the x - and y -polarized OAM_{±1} beams (i.e., OAM_{±1-x} and OAM_{±1-y}) can be synthesized by combining the LP_{11a} and LP_{11b} modes with the same polarization. Fig. 1(d) shows the doughnut-shaped field distributions of the OAM_{±1-x} and OAM_{±1-y} beams as well as the spiral phase structures for their E_x and E_y components.

As a summary, the aforementioned structured light can intuitively be synthesized by exciting two specific power-, polarization- and phased-controlled LP modes. Even though LP modes are well supported in low-index-contrast optical waveguides (such as silica waveguides or fibres), the manipulation of the polarization state and the phase shifting becomes very inconvenient due to the low polarization-selectivity and low thermal-tuning efficiency. In contrast, when using silicon waveguides (which have a high index contrast), it becomes very flexible to manipulate the polarization states, the power ratios, and the phase shifts of the guided modes. As a consequence, here we propose a new PIC structured light generator by incorporating an SOI chip and a silica chip, as shown in Fig. 1(e). In particular, the SOI chip is used for manipulating the polarization states, the power ratios and the phase-shiftings of the guided light, so that three pairs of TE₀/TM₀ modes are generated with flexibly tunable power ratios and phase shifts. The silica chip is used to receive these three pairs of TE₀/TM₀ modes from the SOI chip and then multiplex them to the six quasi LP modes basis sets (i.e. LP_{01-x}, LP_{01-y}, LP_{11a-x}, LP_{11a-y}, LP_{11b-x}, LP_{11b-y}) supported in a silica MBW. With such a configuration, the power ratios and phase shifts of these six LP modes can be controlled freely by tuning the heaters on the SOI chip, and thus the SAM_{±1}, OAM_{±1-x}, and OAM_{±1-y} and RPB/APB beams can selectively be synthesized.

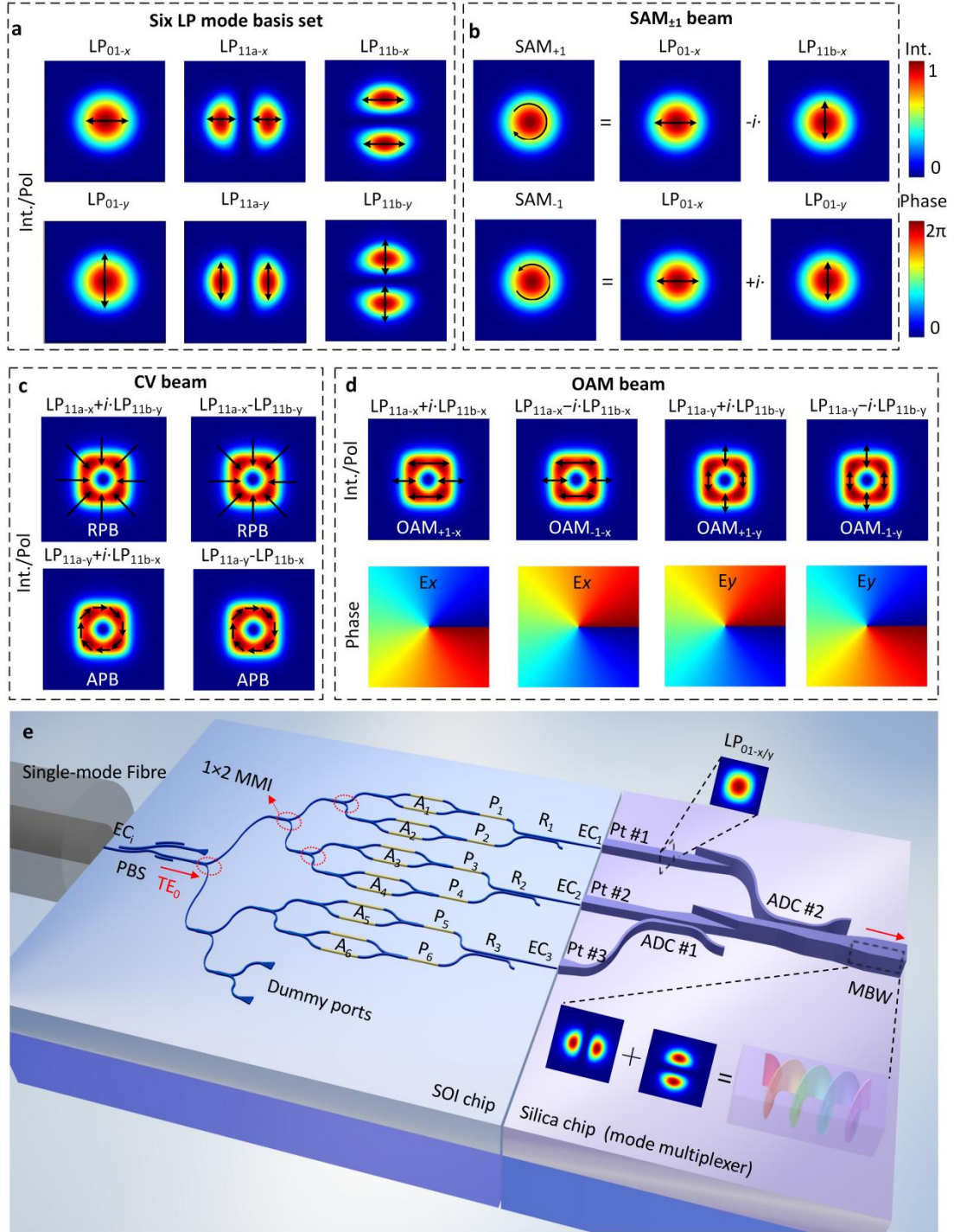


Fig. 1 All-on-chip structured light generator. (a) Six LP mode basis sets at a few-mode fibre or a square silica waveguide, i.e., LP_{01-x} , LP_{01-y} , LP_{11a-x} , LP_{11a-y} , LP_{11b-x} , and LP_{11b-y} modes. (b) Top panel: the SAM_{+1} beam (right-handed circular polarization) is synthesized by the LP_{01-x} and LP_{01-y} modes with a phase difference of $\pi/2$; bottom panel: the SAM_{-1} beam (left-handed circular polarization) is synthesized by the LP_{01-x} and LP_{01-y} modes with a phase difference of $-\pi/2$. (c) The intensity/polarization patterns of the CV beams containing RPB and APB, which both have donut intensity patterns, but are distinguished with radial and azimuthal polarization, respectively. (d) The intensity/polarization patterns and phase structures of the $OAM_{\pm 1-x}$ and $OAM_{\pm 1-y}$ beams. (e) Schematic configuration of the proposed all-on-chip structured light generator incorporating an

SOI chip and a silica chip. Upper inset: the $LP_{01-x/y}$ mode in a silica single mode waveguide; Bottom inset: the $OAM_{\pm 1}$ beam is synthesized as an example by using the LP_{11a} and LP_{11b} modes in a silica multimode bus waveguide (MBW). Operating principle: the light emitted by the fiber to the SOI chip is polarized with a polarization beam splitter (PBS) and then split into six TE_0 modes with a series of 1×2 multimode-interference (MMI) 3-dB couplers. These six TE_0 modes respectively pass through a variable optical attenuator (VOA) and a phase shifter (PS), and then are combined into three pairs of TE_0/TM_0 modes by three polarization splitter-rotators (PSR, R_1 - R_3). These three pairs of TE_0/TM_0 mode are coupled to the LP_{01-x}/LP_{01-y} modes of three silica waveguide ports (Pt #1, Pt #2, and Pt #3) by three edge couplers (ECs, EC_1 - EC_3). Finally, these three pairs of LP_{01-x}/LP_{01-y} modes stimulate the six LP mode basis sets of the MBW through a silica mode multiplexer (containing two adiabatic directional couplers, ADC #1 and ADC #2). One can selectively synthesize the $SAM_{\pm 1}$, $OAM_{\pm 1-x}/OAM_{\pm 1-y}$ beams, as well as the CV beams by controlling the powers and phases of these six LP modes with the six VOAs (A_1 - A_6) and PSs (P_1 - P_6).

As shown in Fig. 2(a), light from a single-mode fibre is coupled to the input port of the SOI chip with the assistance of silicon edge couplers (EC_i) and is polarized to be the TE_0 mode by using a polarization beam splitter (PBS)⁴⁹. The TE_0 mode is then split by using a 1×8 power splitter based on 1×2 multimode-interference (MMI) 3-dB couplers in cascade. Note that there are two dummy ports used for test monitoring. For these six TE_0 modes, there are six variable optical attenuators (VOAs; A_1, A_2, \dots, A_6) to manipulate the power ratios and six phase shifters (PSs; P_1, P_2, \dots, P_6) to manipulate the phase shifts⁵⁰, respectively. These six TE_0 modes with the target power ratios and phase shifts are then recombined to be three TE_0/TM_0 mode-pairs by using three polarization splitter-rotators (PSRs; R_1, R_2, R_3)^{51,52} and output finally from Ports (Pt) #1, #2, and #3, respectively (see Methods). The SOI chip is butt coupled to the silica chip with three ECs (EC_1, EC_2, EC_3), in which way the three pairs of TE_0/TM_0 modes in the three silicon waveguides are coupled respectively to the LP_{01-x}/LP_{01-y} modes of three silica single mode waveguides. Finally, these LP_{01-x}/LP_{01-y} modes are converted and multiplexed to the six LP modes basis sets (i.e. $LP_{01-x}, LP_{01-y}, LP_{11a-x}, LP_{11a-y}, LP_{11b-x}, LP_{11b-y}$) supported in the MBW, by using a polarization-insensitive silica mode multiplexer, which consists of two adiabatic directional couplers (ADCs; ADC #1, ADC #2) in cascade. In detail, the LP_{01} mode launched from Port #1 couples to the LP_{11a} mode of the MBW via ADC #2, while the LP_{01} mode launched from Port #3 couples to the LP_{11a} mode of the MBW via ADC #1 and then is rotated to the LP_{11b} mode with a mode rotator based on a dual-layer silica waveguide. Here the LP_{01} mode launched from Port #2 transmits through these

two ADCs directly. The transmission of the whole PIC structured light generator can be depicted by the transmission matrix method (see Methods). Note that while we have outlined this concept based on the implementation of our silica MBW supporting just six modes, it can be generalised to an arbitrary mode number for both higher OAM orders and TAM control.

2. Fabrication and measurement results

The SOI and silica chips were fabricated separately with their own regular processes. The PBSs and PSRs fabricated on the SOI chip all have a low loss of <1 dB and crosstalk <-15 dB for both TE₀ and TM₀ mode channels (see Methods). The input fibre array, SOI chip, silica chip and FMF were butt-coupled, as shown in Fig. 2(a). Here an ultra-high-NA single mode fibre (HSMF) with a numerical aperture of 0.41 and a core diameter of ~2.4 μm was used for the butt coupling with the SOI chip through an EC, enabling a relatively low coupling loss of ~2 dB for the TE₀ mode in the wavelength range of 1520-1600 nm. The coupling loss between the silicon waveguide and the 4×4 μm² single mode silica waveguide with the help of the same EC is 0.4/1.5 dB for the TE₀/TM₀ modes (see Methods). The silica mode multiplexer has a low on-chip loss of < 0.8 dB and low inter-mode crosstalk of <-14.2 dB for all three modes in the broad wavelength range of 1530-1620 nm⁵³. The SOI chip was wire-bonded onto a printed circuit board (PCB) for electrical control. Fig. 2(b) shows the enlarged views of the SOI and silica chips, and the silica waveguide is labeled with a dotted line. The scanning electron microscope (SEM) images of the PBS, MMI coupler, PSR, and silica waveguide are shown in Fig. 2(c)-(f), respectively.

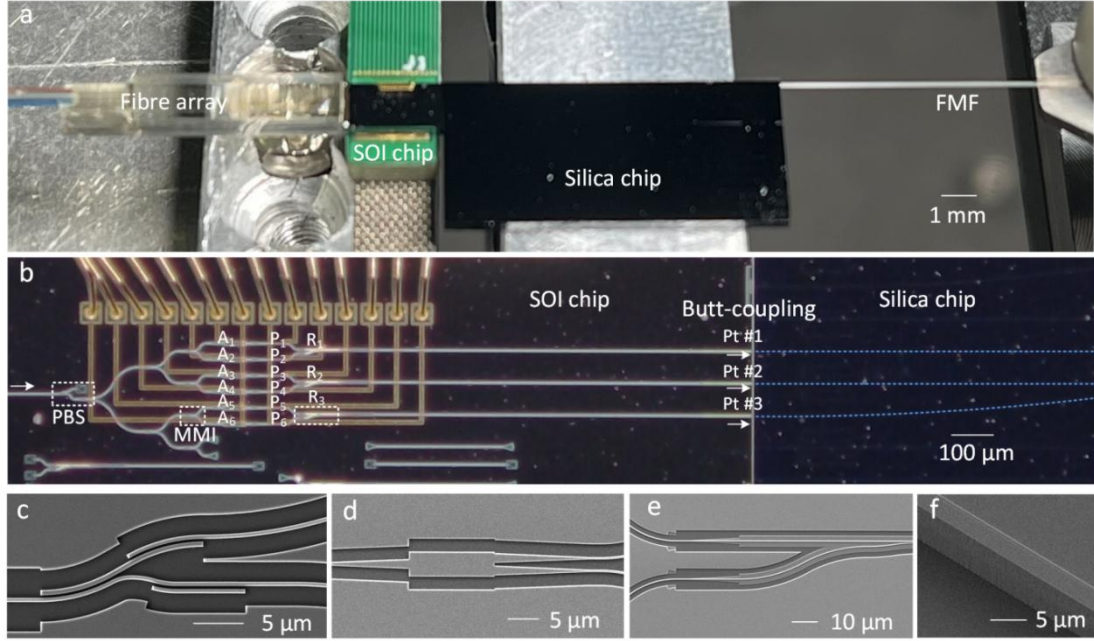


Fig. 2 Images of the fabricated device. (a) The butt-coupled input fibre array, SOI chip, silica chip and FMF. (b) The enlarged view of the butt-coupled SOI chip and silica chip, where the PBS, MMI, VOAs (A_1 - A_6), PSs (P_1 - P_6), PSRs (R_1 - R_3), three ports (Pt #1-#3) are labeled. Scanning electron microscope (SEM) images were given for the (c) PBS, (d) MMI coupler, (e) PSR, and (f) silica waveguide.

3. Generation of the six LP-mode basis sets

A multichannel voltage source (MVS) was used to power the six VOAs and six PSs, so that the power ratios and the phase shifts of these six TE_0/TM_0 channels can be controlled. Fig. 3(a)-3(b) gives the measurement results for the VOAs, showing an excess loss of < 0.6 dB and a maximum extinction ratio of ~ 26 dB at the wavelength of ~ 1580 nm. The thermal tuning of the VOAs and PSs works with a rise time T_r of $11.6 \mu\text{s}$ and a falling time of T_f of $7.1 \mu\text{s}$, enabling fast generation of structured light beams. The amplitude matrix of six LP mode basis sets is given as $\mathbf{A}=[A_1, A_2, A_3, A_4, A_5, A_6]$, where A_m is the amplitude for the m -th mode-channel, and one has $A_m=1$ or 0 by unheating or heating the m -th VOA (VOA_m). As a result, appropriately controlling the VOAs enables to individually excite any one of the LP_{01-x} , LP_{01-y} , LP_{11a-x} , LP_{11a-y} , LP_{11b-x} , and LP_{11b-y} modes in the MBW, as shown in Fig. 3(c) (see Methods). It can be seen that all six LP modes are generated successfully with the desired mode profiles, and the perfect azimuth orthogonality of the LP_{11a} and LP_{11b} modes verifies that the fabricated silica chip performs well. Fig. 3(d) shows the measured transmissions from the input fiber to the output FMF when any one of these six LP

modes is excited individually. It can be seen that the SOI and silica chips for the present structured light generator work well with a low excess loss of about 4-8 dB in a broad wavelength range of 1530-1595 nm (see Methods). Here the excess loss contains the total on-chip losses of about 2 dB, the coupling loss of 0.4/1.5 dB between the silicon and silica chips for x-/y- polarization, and the coupling loss of ~2-4 dB between the silica chip and the few-mode fibre. It is possible to reduce the excess loss further by improving the fabrication.

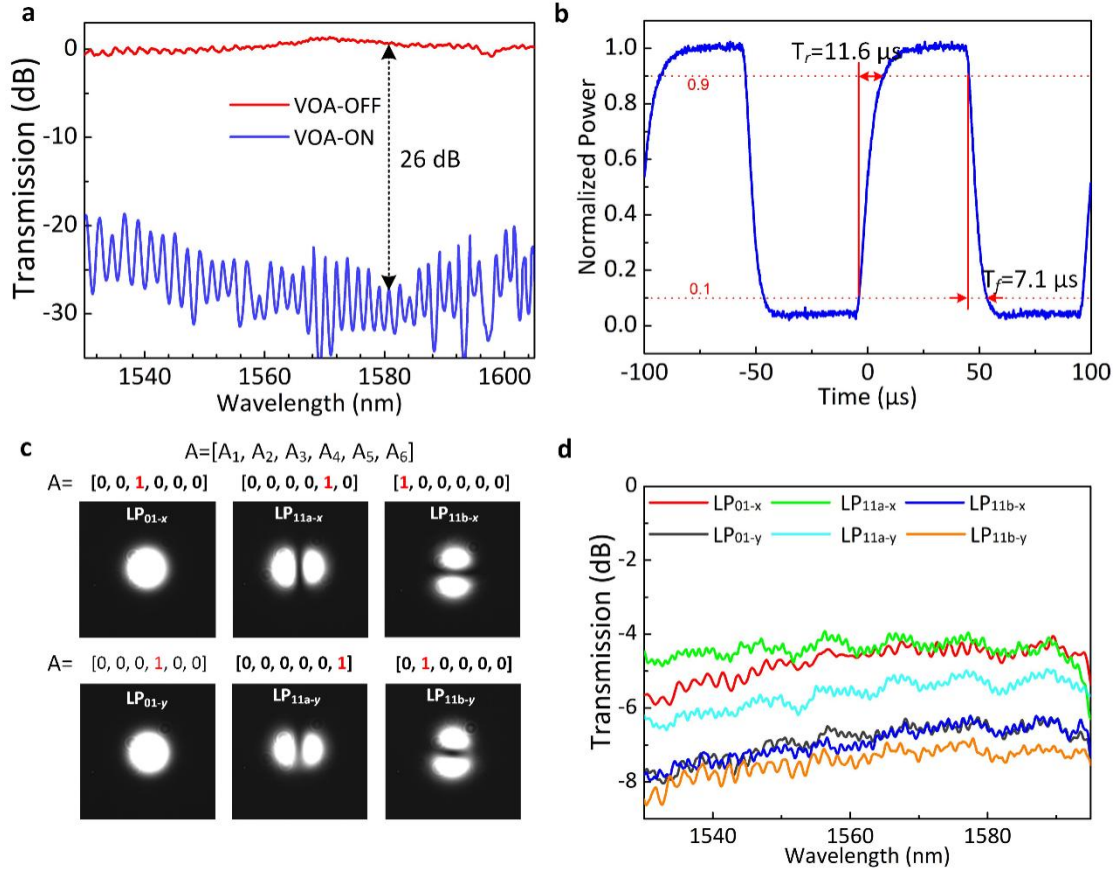


Fig. 3 Characterization of VOAs and the excitation of the six LP mode basis sets. (a) The measured on/off transmissions of the testing VOA fabricated on the same SOI chip, showed a maximum extinction ratio of ~ 26 dB at 1580 nm. **(b)** The measured temporal response of the VOA, exhibits a rise time T_r of 11.6 μs and a falling time T_f of 7.1 μs . **(c)** Any one of six LP-modes excited individually in the MBW by controlling the VOAs to achieve the target amplitude matrix $A = [A_1, A_2, A_3, A_4, A_5, A_6]$ as desired. **(d)** The measured transmissions from the input fiber to the output FMF when any one of these six LP modes is excited individually, show an excess loss of 4-8 dB for all six modes in a broad wavelength range of 1530-1595 nm.

4. Synthesis of SAM

For the generation of the SAM_{±1} beam, the matrix \mathbf{A} was set to $[0, 0, 1, 1, 0, 0]$ so that only the LP_{01-x} and LP_{01-y} modes in the MBW were excited. The modal powers of these two LP modes were balanced by tuning VOA #3 and #4, while their phase difference was tuned to be $\pi/2$ or $-\pi/2$ according to Eq. (1a) by adjusting the bias voltages V_{P3} and V_{P4} applied to the phase shifters P₃ and P₄. The generated SAM_{±1} beam was characterized by using a common quarter-wave plate (QWP) rotation method (see Methods), as shown in Fig. 4(a). Here the phase difference becomes $\pi/2$ and $-\pi/2$ when $V_{P3}=1.95$ V and 3.5 V, respectively. When $V_{P3}=1.95$ V, the mode intensity remained unchanged as the polarizer was rotated with different orientation angles of 45°, 90°, and 135° and 180° (see the black arrows) if no QWP was inserted. In contrast, when a QWP with a horizontal fast axis was placed in front of the polarizer, one observed constructive and destructive interference when the polarizer was 45°- and 135°-orientated, respectively, as shown in the middle panel of Fig. 4(a), indicating that the generated beam carries SAM₊₁ as expected. When further increasing V_{P3} to 3.5 V, constructive and destructive interference respectively happens when the polarizer is 135°- and 45°-orientated, as shown in the bottom panel of Fig. 3(a), indicating the SAM₋₁ beam is generated as desired. Note that the polarization state of the output beam can traverse the whole Poincaré sphere by setting A_2 , A_3 and $V_{P2/3}$ appropriately.

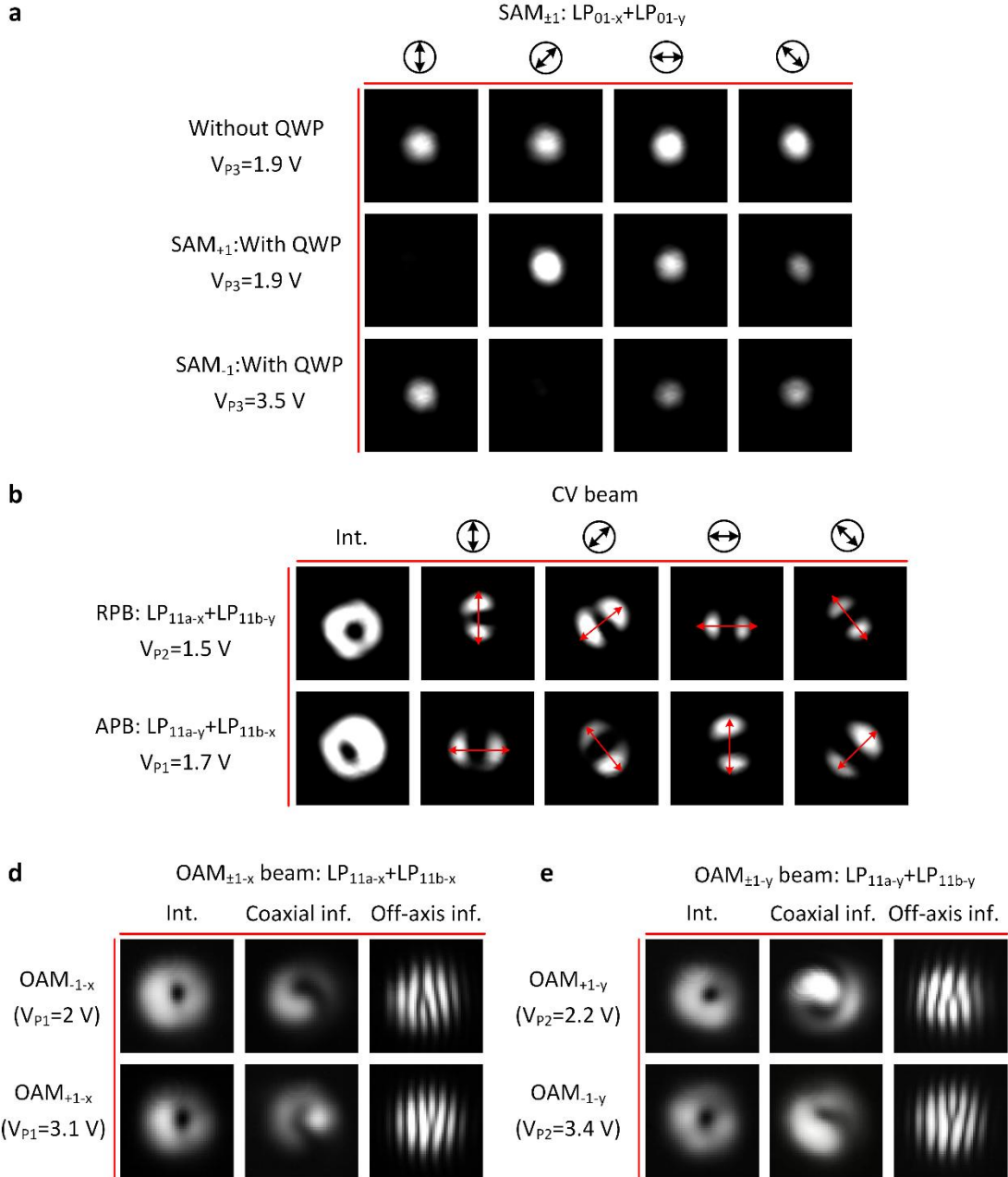


Fig. 4 The experimental synthesis of structured light beams. (a) The $SAM_{\pm 1}$ beam is synthesized by incorporating the LP_{01-x} and LP_{01-y} modes and characterized with the quarter-wave plate (QWP) rotation method. Top panel: the synthesized structured light ($V_{P3}=1.9$ V) passes through a polarizer with different orientations (see the black arrows), and the mode intensity remains unchanged; Middle panel: after inserting a QWP behind the polarizer, constructive interference occurs at the 45° -orientated polarizer, and destructive interference occurs at the 135° -orientated polarizer, confirming the structured light carries SAM_{+1} ; Bottom panel: when further increasing V_{P3} to 3.5 V, the constructive interference and the destructive interference exchange with each other, confirming the structured light carries SAM_{-1} . (b) The CV beams are synthesized by incorporating the LP_{11a} and LP_{11b} modes with different polarizations. Top panel: the RPB is synthesized with the combination of LP_{11a-x} and LP_{11b-y} modes at $V_{P2}=1.5$ V. It has a donut intensity pattern, and maps to an LP_{11} mode with a mode azimuth (yellow arrow) same as the orientation of the polarizer; Bottom panel: the APB is synthesized with the combination of

LP_{11a-y} and LP_{11b-x} modes at $V_{P1}=1.7$ V, and it also has a donut intensity pattern, but maps to an LP₁₁ mode with a mode azimuth angle vertical to the orientation of the polarizer. (c) The OAM_{±1-x} beam is synthesized with the combination of the LP_{11a-x} and LP_{11b-x} modes. The intensity, coaxial interference (inf.), and off-axis interference patterns confirm the generation of OAM_{-1-x} (top panel, at $V_{P1}=2$ V) and OAM_{+1-x} (bottom panel, at $V_{P1}=3.1$ V). (d) The OAM_{±1-y} beam is synthesized with the combination of the LP_{11a-y} and LP_{11b-y} modes. The intensity, coaxial interference (inf.), and off-axis interference pattern confirm the generation of OAM_{-1-x} (top panel, at $V_{P2}=2.2$ V) and OAM_{+1-x} (bottom panel, at $V_{P2}=3.4$ V). (@1550 nm)

5. Synthesis of CV beams

When matrix **A** is set to be [0, 1, 0, 0, 1, 0], the LP_{11a-x} and LP_{11b-y} modes in the MBW are excited simultaneously, and their phase difference can be tuned to 0 or $-\pi/2$, in which case the RPB beam is generated according to Eq. (1b). As shown by the top panel in Fig. 4(b), the synthesized mode field has a donut-shaped intensity when $V_{P2}=1.5$ V. When a polarizer with rotated orientation angles is inserted before the CCD camera (see Methods), a series of LP₁₁ mode fields with different azimuth are achieved (yellow arrow) and the LP₁₁ mode's azimuth is perfectly consistent with the polarizer orientation angles, verifying that the generated CV beam is RPB. In contrast, matrix **A** should be set as [1, 0, 0, 0, 0, 1] to synthesize the APB according to Eq. (1c), in which way the LP_{11a-y} and LP_{11b-x} modes are excited simultaneously. A donut intensity pattern appears when $V_{P1}=1.65$ V, as shown in the bottom panel of Fig. 4(b), while the azimuth of the LP₁₁ mode is perpendicular to the polarizer's transmission axis, as expected.

6. Synthesis of OAM beams

To generate OAM_{±1} beams, the LP_{11a} and LP_{11b} modes with the same polarization should be stimulated according to Eqs. (1d) and (1e). To verify the phase information of the generated OAM beams, an interference measurement method was used (see Methods). For the synthesis of OAM_{+1-x}, the LP_{11a-x} and LP_{11b-x} modes should be excited simultaneously and accordingly matrix **A** is set as [1, 0, 0, 0, 1, 0]. As shown in the top panel of Fig. 4(c), one clearly observes a donut-shaped intensity pattern, a clockwise helical coaxial interference pattern, and a forked off-axis interference pattern when setting $V_{P1}=2.0$ V for achieving the desired $\pi/2$ phase difference between the LP_{11a-x} and LP_{11b-x} modes, which indicates that the OAM₋₁ beam is synthesized successfully. By further increasing the applied voltage V_{P1} to 3.1 V thus adjusting the phase difference to $-\pi/2$, one can also generate the OAM_{+1-x} beam, as shown in the bottom panel of Fig.

4(c). It can be seen that the generated OAM_{+1-x} beam has a donut-shaped intensity pattern, an anti-clockwise helical coaxial interference pattern, and an inverse-forked off-axis interference pattern. Similarly, OAM_{+1-y} and OAM_{-1-y} beams can also be synthesized with the LP_{11a-y} and LP_{11b-y} modes by making the phase difference be $-\pi/2$ and $\pi/2$ when setting $V_{p2}=2.2$ and 3.1 V, respectively, as shown in Fig. 4(d).

7. Extension to TAM

Theoretically, the proposed all-on-chip structured light generator can synthesize a TAM beam that carries both OAM and SAM. A TAM beam is usually described with a higher-order Poincaré (HOP) sphere, in which the basis states are more general orthogonal states that incorporate both SAM and OAM^{12,54}. In our case, a TAM beam can be described as follows

$$TAM = (O_x + e^{-i\varphi} \cdot O_y)/\sqrt{2}, \quad (2)$$

in which

$$O_x = (LP_{11a-x} + e^{-i\theta_1} \cdot LP_{11b-x})/\sqrt{2}, \quad (2-a)$$

$$O_y = (LP_{11a-y} + e^{-i\theta_2} \cdot LP_{11b-y})/\sqrt{2}. \quad (2-b)$$

Therefore, a TAM beam can be synthesized with four LP_{11} modes (i.e., LP_{11a-x} , LP_{11a-y} , LP_{11b-x} , LP_{11b-y}) and carries three phase terms (i.e., θ_1 , θ_2 , and φ). More details about these phase terms are explained below.

(1) θ_1 is the phase difference between the LP_{11a-x} and LP_{11b-x} modes, determining the phase structure of the E_x component of the TAM beam.

(2) θ_2 is the phase difference between the LP_{11a-y} and LP_{11b-y} modes, determining the phase structure of the E_y component of the TAM beam.

(3) φ is the phase difference of the terms O_x and O_y , determining the polarization state of the TAM beam.

As an example, Fig. 5 shows some of the synthesized TAMs, showing their intensity/polarization patterns, and the phase structures of their E_x and E_y components. In these examples, the phase terms θ_1 and θ_2 are chosen to be $\pm\pi/2$ so that both E_x and E_y components carry $OAM_{\pm 1}$; while φ is appropriately chosen to produce the linear polarization (e.g., $[\theta_1, \theta_2, \varphi]=[\pi/2, \pi/2, \pi/2]$ or $[-\pi/2, -\pi/2, -\pi/2]$) or the vortex-like polarization (e.g., $[\theta_1, \theta_2, \varphi]=[\pi/2, \pi/2, 0]$ or $[-\pi/2, \pi/2, \pi/2]$), respectively. For the structured light with $[\theta_1, \theta_2, \varphi]=[\pi/2, \pi/2, 0]$ considered as an

example, it has clockwise vortex-like polarization distribution, and the components of E_x and E_y carry OAM_{+1} , OAM_{-1} , respectively. By appropriately choosing the phase differences $[\theta_1, \theta_2, \varphi]$, one can traverse the entire HOP sphere and synthesize the desired light beams carrying $OAM_{\pm 1-x}$, $OAM_{\pm 1-y}$, and SAM^{41} . In order to generate the aforementioned TAM beams, definitely the powers and phases of these four LP_{11} modes should be accuracy adjusted and one should minimize the thermal crosstalk on the SOI chip.

$$TAM = (LP_{11a-x} + e^{-i\theta_1} \cdot LP_{11b-x})/2 + e^{-i\varphi} \cdot (LP_{11a-y} + e^{-i\theta_2} \cdot LP_{11b-y})/2$$

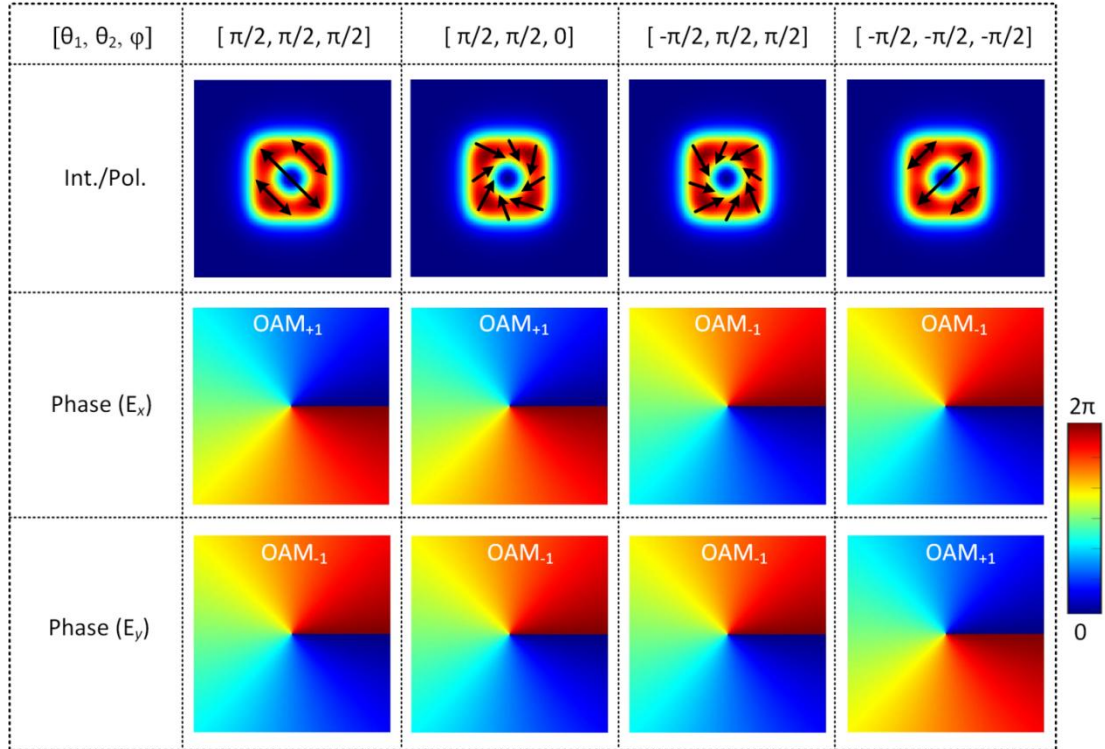


Fig. 5 The synthesis of the TAM beams. The simulated intensity/polarization patterns, phase structure of the E_x component, and phase structure of the E_y component of the synthesized TAM beam by stimulating LP_{11a-x} , LP_{11a-y} , LP_{11b-x} , LP_{11b-y} modes with different phases $[\theta_1, \theta_2, \varphi]$. When $[\theta_1, \theta_2, \varphi]=[\pi/2, \pi/2, \pi/2]$, the structured light has a donut intensity, 135° linear polarization and carries OAM_{+1-x} and OAM_{+1-y} ; When $[\theta_1, \theta_2, \varphi]=[\pi/2, \pi/2, 0]$, the structured light has a donut intensity, clockwise-vortex polarization and carries OAM_{+1-x} and OAM_{+1-y} ; When $[\theta_1, \theta_2, \varphi]=[-\pi/2, \pi/2, \pi/2]$, the structured light has a donut intensity, anticlockwise-vortex polarization, and carries OAM_{-1-x} and OAM_{-1-y} ; When $[\theta_1, \theta_2, \varphi]=[-\pi/2, -\pi/2, -\pi/2]$, the structured light has a donut intensity, 45° linear polarization, and carries OAM_{-1-x} and OAM_{+1-y} .

Discussion

In summary, we have demonstrated an all-on-chip reconfigurable structured light generator by incorporating an SOI chip with a silica chip. Our work advances the nascent field of PICs for

structured light creation, showing how to both create and control the light all on-chip without the clumsy external free-space conversion (which negates the very benefit of starting on-chip in the first place). We demonstrate its power by going beyond the state-of-the-art and showing full angular momentum control, from scalar orbital angular momentum (OAM) to vectorial combinations, made possible by full polarisation control. Not only do we create this on-chip, but we also keep it there, with direct control and delivery through a waveguide. Further, our device has a fibre input and fibre output for a truly integrated, compact and reconfigurable solution, showing excellent performance in modal spectrum, wavelength spectrum and speed. We believe that this makes our solution idea for applications such as mode division multiplexing in fibre, fibre sensing with structured light and on-chip quantum technologies based on the spatial modes of light.

The proposed structured light generator can synthesize more complex total angular momentum beams and it can be extended to generate higher-order structured light beams by increasing the modal capacity of the silica mode multiplexer and the output number of the SOI chip. Compared with the methods reported previously on-chip generating structured light, the scheme proposed here shows a prominent advantage of versatility, broad bandwidth, and high conversion efficiency. Since the silica MBW can be butt-coupled efficiently to an FMF with a low coupling loss of <2 dB or less for all six LP modes by using the proposed multimode segmented waveguide⁵³, the structured light beams synthesized by the present all-on-chip generator can be guided into an OAM fibre conveniently for remote applications. Further improvement should be attention to further minimizing the excess loss, which is possible by introducing a variable power splitter⁵⁵ as well as adopting a compact architecture.

Materials and Methods

1. Silicon photonic chip design

Figure. S1(a) shows the schematic configuration of the SOI chip that produces three pairs of TE₀/TM₀ modes whose power ratios and phase shifts can be tuned thermally. The SOI chip consists of a PBS, seven 1×2 MMI 3-dB couplers, six variable optical attenuators (VOAs; A₁, A₂, ..., A₆), six phase shifters (PSs; P₁, P₂, ..., P₆), three PSRs (R₁, R₂, R₃), and four ECs (EC_{*i*},

EC₁, EC₂, EC₃). Fig. S1(b) shows the cross-section of the silicon photonic waveguide, which has a 220-nm-thick silicon core layer surrounded by silica, and a metal micro-heater is located on the top with a separation of $h_g=1.5\ \mu\text{m}$ to balance the heating efficiency and optical absorption loss. The PBS used here is designed based on the bent directional coupler as shown in Fig. S1(c) proposed in⁴⁹. The PSR used here works on the principle of mode hybridness of the tapered ridge waveguide, and a directional coupler is further used to separate the TE₀ and TM₀ modes, as shown in Fig. S1(d)^{51,52}. The 1×2 3-dB coupler is designed based on MMI as shown in Fig. S1(e). The VOAs are designed based on a symmetric 1×1 Mach-Zender interferometer (MZI) as shown in Fig. S1(f). The designed phase shifters are shown in Fig. S1(g), which utilizes the effective thermo-optical coefficient difference between the TE₀ and TM₀ modes in a silicon photonic waveguide, and the waveguide width of $0.45\ \mu\text{m}$ is chosen to balance the thermal efficiency and transmission loss⁵⁰. The EC based on an inverse taper structure at the two ends of the SOI is used for the butt coupling between the SOI chip and HSMF or silica single mode waveguide, as shown in Fig. S1(h). The inverse taper is linearly tapered from 0.45 to $0.16\ \mu\text{m}$, thus well matching the mode field of the HSMF or silica single mode waveguide. The key parameters of the designed silicon components are summarized in Table S1.

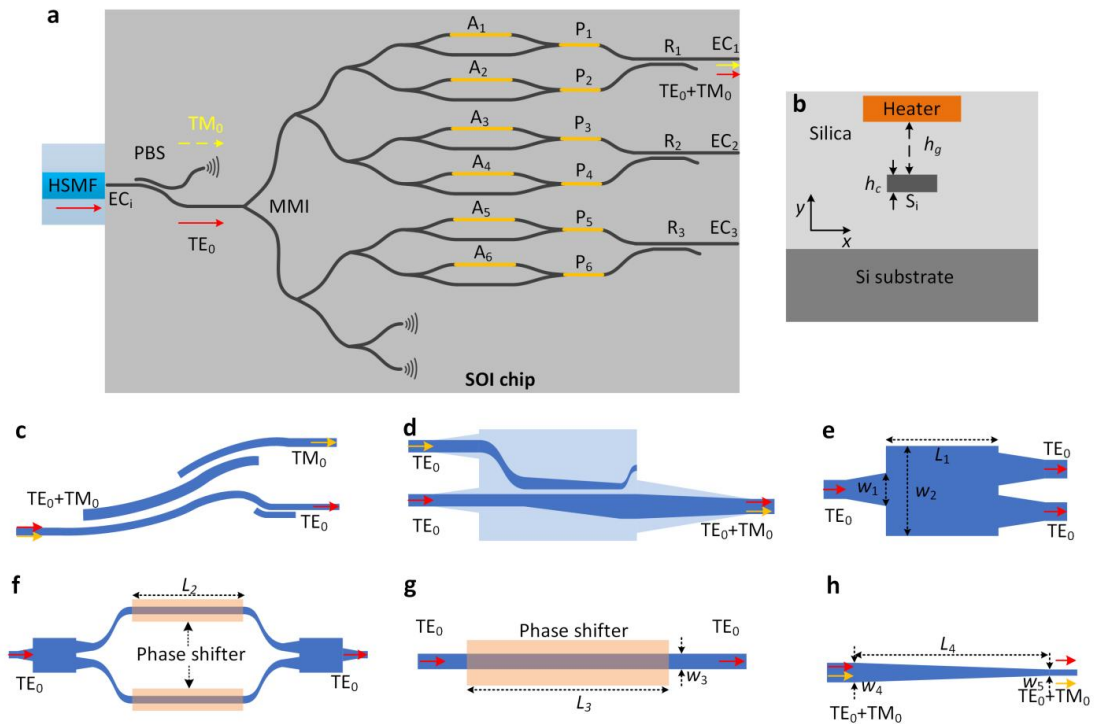


Figure S1. Silicon photonic chip. (a) Schematic configuration of the SOI chip, which consists of a polarization beam splitter (PBS), seven 1×2 3-dB multimode interference (MMI) couplers, six

variable optical attenuators (VOAs; A_1, A_2, \dots, A_6), six phase shifters (PSs; P_1, P_2, \dots, P_6), three polarization-splitter rotators (PSRs, R_1, R_2, R_3), and four edge couplers (EC; EC_i, EC_1, EC_2, EC_3). **b** The silicon waveguide cross-section. The schematic configuration of the **(c)** PBS, **(d)** PSR, **(e)** 1×2 MMI coupler, **(f)** VOA, **(g)** PS, and **(h)** EC.

TABLE S1. The key parameters of the designed silicon photonic devices.

Parameters	w_1	w_2	w_3	w_4	w_5	L_1	L_2	L_3	L_4
Value (μm)	1.6	4	0.45	0.45	0.16	13.75	50	50	180

2. Silica mode multiplexer design

The three-channel silica mode multiplexer consists of two cascaded adiabatic directional couplers (ADC #1, ADC #2), a mode rotator and has a total length $L=6000 \mu\text{m}$ as shown in Fig. S2(a). The silica mode multiplexer is polarization-insensitive due to the low birefringence and low index contrast. The inset of Fig. S2(a) shows the cross-section of the silica waveguide, whose index contrast is about 1.5%. In particular, the silica waveguides are designed with two different heights, i.e., $h_1=6.5 \mu\text{m}$ and $h_2=4$, to realize efficient conversion of the LP_{01} and LP_{11b} modes which have different mode-field symmetry⁵⁶. The core sizes of the single mode input waveguide and multimode output waveguide are $4.0 \times 4.0 \mu\text{m}^2$ and $6.5 \times 6.5 \mu\text{m}^2$, respectively. At the output port, the silica multimode bus waveguide (MBW) can couple to the FMF with high efficiency and low crosstalk for the applications. The operation principle of the mode multiplexer is shown with details in Fig. S2(b). Here the LP_{01} mode launched into Pt #1 couples to the LP_{11a} mode of the MBW via ADC #2; the LP_{01} mode launched into Pt #2 passes through the two ADCs directly; meanwhile, the LP_{01} mode launched into Pt #3 couples to the LP_{11a} mode of the MBW via ADC #1 first and then rotates to LP_{11b} mode with a mode rotator based on the tilt-etched dual-layer waveguide. The simulated transmissions for the lights launched into Pt #2, Pt #3, and Pt #1 are shown in Fig. S2(b, c, d), respectively, while the insets show the corresponding light propagation for the operation at the wavelength of 1550 nm. The simulation results show the designed mode multiplex has an ultra-low loss less than 0.04 dB and crosstalk less than -32 dB for the LP_{01} , LP_{11a} , and LP_{11b} modes in the wavelength range of 1500-1600 nm. The ultra-low loss and low crosstalk can be attributed to the principle of adiabatic mode evolution in the designed ADCs.

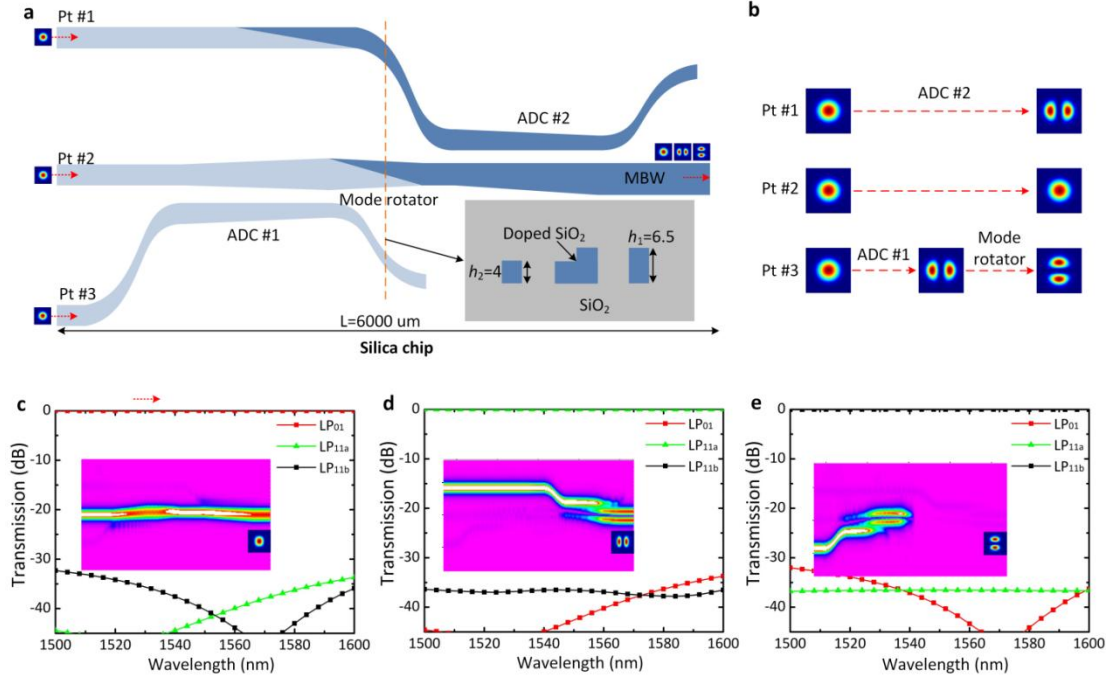


Figure S2. Silica chip. (a) Schematic configuration of the silica mode multiplexer, consisting of three input ports (Pt #1, Pt #2, Pt #3), two adiabatic directional couplers (ADC #1 and ADC #2), a mode rotator, and an output silica multimode bus waveguide (MBW). The inset shows the cross-section of the silica waveguide, it has a doped silica core and a pure silica cladding, while the silica single mode waveguide and multimode waveguide are designed with the core heights of $h_2=4 \mu\text{m}$ and $h_1=6.5 \mu\text{m}$, respectively. (b) Operation principle: the LP_{01} mode launched into Pt #1 couples to the LP_{11a} mode of the MBW via ADC #2; the LP_{01} mode launched into Pt #2 passes through the two ADCs directly; the LP_{01} mode launched into Pt #3 is coupled to the LP_{11a} mode of the MBW via ADC #1 first and is then rotated to the LP_{11b} mode with a mode rotator based on the tilt-etched dual-layer waveguide. Simulated transmissions when light launched into (c) Pt #2, (d) Pt #1, and (e) Pt #3, the insets show the corresponding light propagation at 1550 nm.

3. Transmission matrix

The transmission of the structured light generator can be depicted by the following transmission matrix:

$$E_{out} = C_P C_A E_{in}, \quad (3)$$

in which E_{in} is the excited six LP modes basis sets, C_A is the amplitude matrix controlled by the six VOAs, and C_P is the phase matrix controlled by the six PSs. They are given as:

$$E_{in} = [\text{LP}_{11a-x} \quad \text{LP}_{11a-y} \quad \text{LP}_{01-x} \quad \text{LP}_{01-y} \quad \text{LP}_{11b-x} \quad \text{LP}_{11b-y}]^T, \quad (3-a)$$

$$C_A = \begin{bmatrix} A_1 & 0 & 0 & 0 & 0 & 0 \\ 0 & A_2 & 0 & 0 & 0 & 0 \\ 0 & 0 & A_3 & 0 & 0 & 0 \\ 0 & 0 & 0 & A_4 & 0 & 0 \\ 0 & 0 & 0 & 0 & A_5 & 0 \\ 0 & 0 & 0 & 0 & 0 & A_6 \end{bmatrix} \quad (3-b)$$

$$C_p = [e^{-i\varphi_1} \quad e^{-i\varphi_2} \quad e^{-i\varphi_3} \quad e^{-i\varphi_4} \quad e^{-i\varphi_5} \quad e^{-i\varphi_6}] \quad (3-c)$$

4. Fabrication

The SOI wafer used here has a 3- μm -thick buffer layer and a 220-nm-thick top-silicon core layer. The processes of electron beam lithography (EBL) and inductively coupled plasma (ICP) were used to form the bi-level ridge waveguides with a slab thickness of 70 nm. A 2.3- μm -thick silica upper cladding was deposited with the plasma-enhanced chemical vapor deposition (PECVD) process, and the 300-nm Cr/Ti metal layer was embedded into the cladding as the heater.

The silica chip was fabricated with a silica wafer with a silicon substrate, a 10- μm -thick silica buffer layer, and a 6.5- μm -thick doped silica-core layer. Here the index contrast of silica waveguides is about 1.5%. The silica core layer was etched with the Cr mask by using the inductively coupled plasma (ICP) process. Finally, a 15- μm silica upper cladding was formed by using the flame hydrolysis deposition (FHD) technology.

5. Measurement

Figure S3(a) shows the experimental setup for mode field detection. Here a tunable laser (TL) @1550 nm and a fibre polarization controller (PC) connected with an HSMF were used at the input side to be butt-coupled efficiently to the SOI chip, while the SOI chip was then butt-coupled to the silica chip. Finally, the light output from the silica MBW was collimated by a 20 \times objective, then passed through a QWP (with a horizontal fast axis), a polarizer, and was finally captured with a CCD camera. A multichannel voltage source (MVS) was used to power the six VOAs and six PSs, so that the power ratios and the phase shifts of these six TE₀/TM₀ channels can be controlled. Fig. S3(b) shows the experimental setup for measuring the transmission of generated six LP-mode basis sets. Here amplified spontaneous emission (ASE) was used as a light source, and the output LP modes were received with a few-mode fibre (FMF) and sent into an optical spectrum analyzer (OSA).

The interference setup for detecting the synthesized OAM light beam is shown in Fig. S3(c). Here light from a tunable laser was divided into two parts with a power ratio of 50%:50% through a fibre 3-dB coupler. One part was sent into the SOI chip and used as the signal beam, and the other one was used as the reference Gaussian beam for interference. The signal light passed through the chips and finally was expanded with a 20× Objective, while the reference Gaussian beam was collimated with a fibre collimator. When the signal light and the reference Gaussian beam were combined with a nonpolarizing beam splitter (NPBS), and the generated interference pattern was then captured with a CCD camera. The power ratio of these two routes was balanced with two optical attenuators, and their polarization states were calibrated with two fibre PCs.

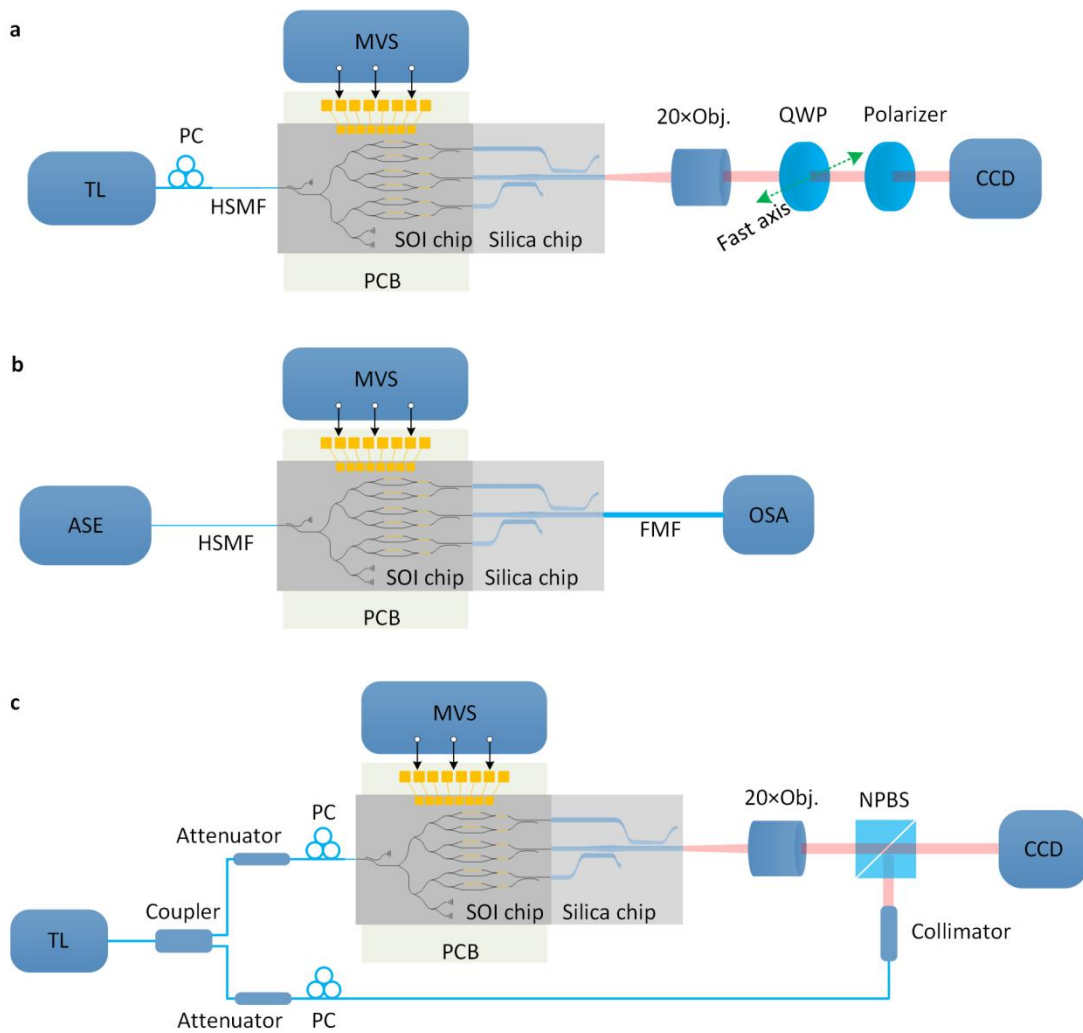


Figure S3. Measurement experiment setup. (a) Experiment setup for mode field detection, (b) Experiment setup for the measurement of mode transmissions. (c) The experiment setup for detecting the OAM beams. TL: tunable laser, ASE: amplified spontaneous emission, MVS: multichannel voltage source, PCB: printed circuit board, HSMF: high-NA single mode fibre, PC: polarization controller, MVS: multi-channel voltage source, FMF: few-mode fibre, OSA: optical

spectrum analyzer, QWP: quarter-wave plate, NPBS: nonpolarizing beam splitter, CCD: charge coupled device.

6. Butt-coupling loss and PBS, PSR performances

The HSMF and SOI waveguide coupling was achieved with a silicon EC based on an inverse taper waveguide. The measured coupling loss for each HSMF-SOI facet is shown in Fig. S4(a), and it is 2 dB for the TE_0 mode in the 1520-1600 nm wavelength range. The coupling between the SOI waveguide and a $4 \times 4 \mu\text{m}^2$ single mode silica waveguide is also achieved with the same EC. Fig. S4(b) shows the measured SOI-Silica butt-coupling loss, which is about 0.4/1.5 dB for the TE_0/TM_0 modes in the wavelength range around 1560 nm.

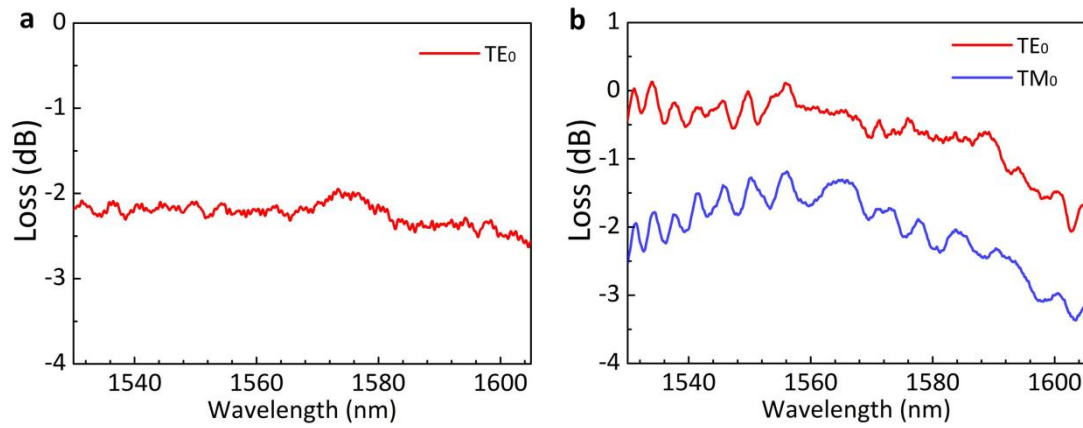


Figure S4. (a) The measured butt-coupling loss for the TE_0 mode between an HSMF and a silicon waveguide; (b) The measured butt-coupling losses for TE_0/TM_0 modes between a silicon waveguide and a silica waveguide.

The measure results for the testing silicon PBS and PSR fabricated on the same chip are shown in Fig. S5(a, b), respectively. The PBS has a low loss of <1 dB and low crosstalk <-15 dB for both the TE_0 and TM_0 modes. The PSR has a low loss of <1 dB and low crosstalk <-15 dB for both the TE_0 and TM_0 modes.

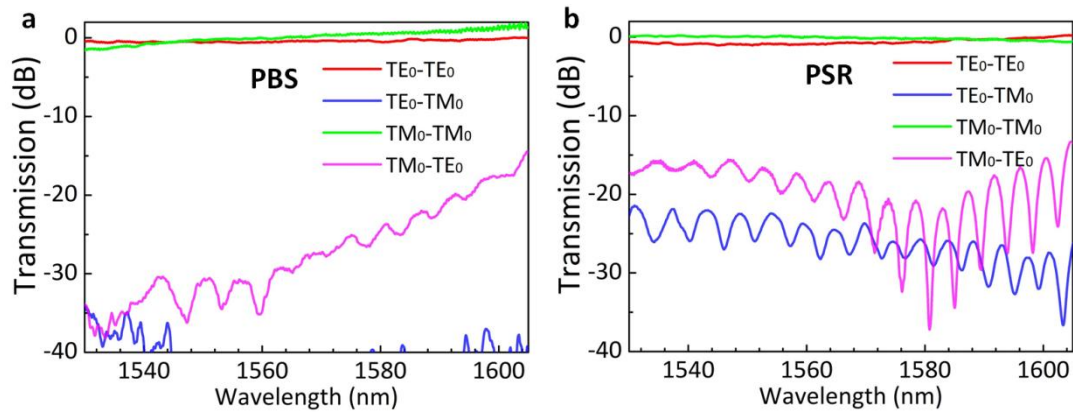


Figure S5. The measured transmissions for (a) the PBS, (b) the PSR.

Data availability statement

All data are available in the main text or the supplementary materials.

Conflict of interest

All other authors declare they have no competing interests.

Acknowledgments

This work is supported by National Natural Science Foundation of China (NSFC) (62375238, 92150302, U23B2047, and 62321166651), Zhejiang Provincial Major Research and Development Program under Grant 2021C01199, The Fundamental Research Funds for the Central Universities, The Leading Innovative and Entrepreneur Team Introduction Program of Zhejiang (2021R01001).

Author contributions

W. K. Z. and D. X. D. conceived the idea. W. K. Z and X. L. Y. contributed equally to this work. W. K. Z and R. R. L. designed and fabricated the silicon chip. X. L. Y. designed and fabricated the silica chip. K. Z and X. L. Y. built the setup and carried out the experiment. All authors discussed the results and contributed to the manuscript. W. K. Z, X. L. Y., D. X. D. and A. F. wrote the manuscript. D. X. D. supervised the project.

References

1. Forbes, A., De Oliveira, M. & Dennis, M. R. Structured light. *Nat. Photonics* **15**, 253–262 (2021).
2. Wan, C., Cao, Q., Chen, J., Chong, A. & Zhan, Q. Toroidal vortices of light. *Nat. Photon.* (2022) doi:10.1038/s41566-022-01013-y.
3. Mao, D. *et al.* Generation of polarization and phase singular beams in fibers and fiber lasers. *Adv. Photon.* **3**, (2021).
4. Forbes, A., Ramachandran, S. & Zhan, Q. Photonic angular momentum: progress and perspectives. *Nanophotonics* **11**, 625–631 (2022).
5. Sarmiento-Merenguel, J. D. *et al.* Demonstration of integrated polarization control with a 40 dB range in extinction ratio. *Optica* **2**, 1019 (2015).
6. Lin, Z. *et al.* High-performance polarization management devices based on thin-film lithium niobate. *Light Sci Appl* **11**, 93 (2022).
7. Dong, J. & Chiang, K. S. Temperature-Insensitive Mode Converters With CO₂-Laser Written Long-Period Fiber Gratings. *IEEE Photon. Technol. Lett.* **27**, 1006–1009 (2015).
8. Mao, D. *et al.* All-fiber radially/azimuthally polarized lasers based on mode coupling of tapered fibers. *Opt. Lett.* **43**, 1590 (2018).
9. Xie, Z. *et al.* Integrated (de)multiplexer for orbital angular momentum fiber communication. *Photon. Res.* **6**, 743 (2018).
10. Ni, J. *et al.* Multidimensional phase singularities in nanophotonics. *Science* **374**, eabj0039 (2021).
11. Holleczek, A., Aiello, A., Gabriel, C., Marquardt, C. & Leuchs, G. Classical and quantum properties of cylindrically polarized states of light. *Opt. Express* **19**, 9714 (2011).
12. Naidoo, D. *et al.* Controlled generation of higher-order Poincaré sphere beams from a laser. *Nature Photon* **10**, 327–332 (2016).
13. Min, C. *et al.* Focused plasmonic trapping of metallic particles. *Nat Commun* **4**, 2891 (2013).
14. Zhang, Y. *et al.* Plasmonic tweezers: for nanoscale optical trapping and beyond. *Light Sci Appl* **10**, 59 (2021).
15. Stilgoe, A. B., Nieminen, T. A. & Rubinsztein-Dunlop, H. Controlled transfer of transverse orbital angular momentum to optically trapped birefringent microparticles. *Nat. Photon.* **16**, 346–351 (2022).
16. Xie, X., Chen, Y., Yang, K. & Zhou, J. Harnessing the Point-Spread Function for High-Resolution Far-Field Optical Microscopy. *Phys. Rev. Lett.* **113**, 263901 (2014).
17. Mao, D. *et al.* Optical vortex fiber laser based on modulation of transverse modes in two mode fiber. *APL Photonics* **4**, 060801 (2019).
18. Wang, J. *et al.* Terabit free-space data transmission employing orbital angular momentum

- multiplexing. *Nature Photon* **6**, 488–496 (2012).
19. Wang, J. *et al.* Orbital angular momentum and beyond in free-space optical communications. *Nanophotonics* **11**, 645–680 (2022).
 20. Dholakia, K. & Čižmár, T. Shaping the future of manipulation. *Nature Photon* **5**, 335–342 (2011).
 21. Paterson, L. *et al.* Controlled Rotation of Optically Trapped Microscopic Particles. *Science* **292**, 912–914 (2001).
 22. Roy, B., Ghosh, N., Banerjee, A., Gupta, S. D. & Roy, S. Manifestations of geometric phase and enhanced spin Hall shifts in an optical trap. *New J. Phys.* **16**, 083037 (2014).
 23. Fang, L., Padgett, M. J. & Wang, J. Sharing a Common Origin Between the Rotational and Linear Doppler Effects. *Laser & Photonics Reviews* **11**, 1700183 (2017).
 24. Liu, J. & Wang, J. Demonstration of polarization-insensitive spatial light modulation using a single polarization-sensitive spatial light modulator. *Sci Rep* **5**, 9959 (2015).
 25. Maurer, C., Jesacher, A., Bernet, S. & Ritsch-Marte, M. What spatial light modulators can do for optical microscopy. *Laser & Photon. Rev.* **5**, 81–101 (2011).
 26. Liu, T., Chen, S.-P. & Hou, J. Selective transverse mode operation of an all-fiber laser with a mode-selective fiber Bragg grating pair. *Opt. Lett.* **41**, 5692 (2016).
 27. Zhao, H., Wang, P., Yamakawa, T. & Li, H. All-fiber second-order orbital angular momentum generator based on a single-helix helical fiber grating. *Opt. Lett.* **44**, 5370 (2019).
 28. Wong, G. K. L. *et al.* Excitation of Orbital Angular Momentum Resonances in Helically Twisted Photonic Crystal Fiber. *Science* **337**, 446–449 (2012).
 29. Wang, T. *et al.* High-order mode direct oscillation of few-mode fiber laser for high-quality cylindrical vector beams. *Opt. Express* **26**, 11850 (2018).
 30. Chen, R. *et al.* High efficiency all-fiber cylindrical vector beam laser using a long-period fiber grating. *Opt. Lett.* **43**, 755 (2018).
 31. Fu, S. *et al.* Orbital angular momentum comb generation from azimuthal binary phases. *Adv. Photon. Nexus* **1**, (2022).
 32. Forbes, A. Structured Light from Lasers. *Laser & Photonics Reviews* **13**, 1900140 (2019).
 33. Forbes, A., Mkhumbuza, L. & Feng, L. Orbital angular momentum lasers. *Nat Rev Phys* (2024) doi:10.1038/s42254-024-00715-2.
 34. Carlon Zambon, N. *et al.* Optically controlling the emission chirality of microlasers. *Nat. Photonics* **13**, 283–288 (2019).
 35. Shao, Z., Zhu, J., Zhang, Y., Chen, Y. & Yu, S. On-chip switchable radially and azimuthally polarized vortex beam generation. *Opt. Lett.* **43**, 1263 (2018).
 36. Zhang, Z. *et al.* Tunable topological charge vortex microlaser. *Science* **368**, 760–763 (2020).
 37. Zhang, Z. *et al.* Spin–orbit microlaser emitting in a four-dimensional Hilbert space. *Nature*

612, 246–251 (2022).

38. Strain, M. J. *et al.* Fast electrical switching of orbital angular momentum modes using ultra-compact integrated vortex emitters. *Nat Commun* **5**, 4856 (2014).
39. Devlin, R. C., Ambrosio, A., Rubin, N. A., Mueller, J. P. B. & Capasso, F. Arbitrary spin-to-orbital angular momentum conversion of light. *Science* **358**, 896–901 (2017).
40. Li, G. *et al.* Spin-Enabled Plasmonic Metasurfaces for Manipulating Orbital Angular Momentum of Light. *Nano Lett.* **13**, 4148–4151 (2013).
41. Zhou, N. *et al.* Ultra-compact broadband polarization diversity orbital angular momentum generator with $3.6 \times 3.6 \mu\text{m}^2$ footprint. *Sci. Adv.* **5**, eaau9593 (2019).
42. Zheng, S., Zhao, Z. & Zhang, W. Versatile generation and manipulation of phase-structured light beams using on-chip subwavelength holographic surface gratings. *Nanophotonics* **12**, 55–70 (2023).
43. Cai, X. *et al.* Integrated Compact Optical Vortex Beam Emitters. *Science* **338**, 363–366 (2012).
44. Zhang, C. *et al.* High Efficiency Grating Coupler for Coupling between Single-Mode Fiber and SOI Waveguides. *Chinese Phys. Lett.* **30**, 014207 (2013).
45. Raval, M., Poulton, C. V. & Watts, M. R. Unidirectional waveguide grating antennas with uniform emission for optical phased arrays. *Opt. Lett.* **42**, 2563 (2017).
46. Zhong, H. *et al.* Gigahertz-rate-switchable wavefront shaping through integration of metasurfaces with photonic integrated circuit. *Adv. Photon.* **6**, (2024).
47. Bütow, J., Eismann, J. S., Sharma, V., Brandmüller, D. & Banzer, P. Generating free-space structured light with programmable integrated photonics. *Nat. Photon.* **18**, 243–249 (2024).
48. Won, R. On-chip ultrafast wavefront shaping. *Nat. Photon.* **18**, 213–213 (2024).
49. Wu, H., Tan, Y. & Dai, D. Ultra-broadband high-performance polarizing beam splitter on silicon. *Opt. Express* **25**, 6069 (2017).
50. Zhao, W. *et al.* Ultracompact silicon on-chip polarization controller. *Photon. Res.* **12**, 183 (2024).
51. Zhao, W. *et al.* 96-Channel on-chip reconfigurable optical add-drop multiplexer for multidimensional multiplexing systems. *Nanophotonics* **11**, 4299–4313 (2022).
52. Yin, Y., Li, Z. & Dai, D. Ultra-Broadband Polarization Splitter-Rotator Based on the Mode Evolution in a Dual-Core Adiabatic Taper. *J. Lightwave Technol.* **35**, 2227–2233 (2017).
53. X. Yi, W. Zhao, L. Zhang, Y. Shi, and D. Dai, “Efficient mode coupling/(de)multiplexing between a few-mode fiber and a silicon photonic chip,” *Photon. research*, submitted.
54. Bomzon, Z., Kleiner, V. & Hasman, E. Pancharatnam–Berry phase in space-variant polarization-state manipulations with subwavelength gratings. *Opt. Lett.* **26**, 1424 (2001).
55. Song, L. *et al.* Toward calibration-free Mach–Zehnder switches for next-generation silicon photonics. *Photon. Res.* **10**, 793 (2022).

56. Zhao, W. K., Chen, K. X. & Wu, J. Y. Broadband Mode Multiplexer Formed With Non-Planar Tapered Directional Couplers. *IEEE Photon. Technol. Lett.* **31**, 169–172 (2019).